

Optical and magnetic resonance spectra of inorganic molecular crystals-uranium borohydride $[U(BH_4)_4]$ in hafnium borohydride $[Hf(BH_4)_4]$

E. R. Bernstein and T. A. Keiderling

Citation: *The Journal of Chemical Physics* **59**, 2105 (1973); doi: 10.1063/1.1680297

View online: <http://dx.doi.org/10.1063/1.1680297>

View Table of Contents: <http://aip.scitation.org/toc/jcp/59/4>

Published by the [American Institute of Physics](#)



**COMPLETELY
REDESIGNED!**

**PHYSICS
TODAY**

Physics Today Buyer's Guide
Search with a purpose.

Optical and magnetic resonance spectra of inorganic molecular crystals—uranium borohydride $[\text{U}(\text{BH}_4)_4]$ in hafnium borohydride $[\text{Hf}(\text{BH}_4)_4]^*,\dagger$

E. R. Bernstein and T. A. Keiderling[‡]

Department of Chemistry, Princeton University, Princeton, New Jersey 08540

(Received 16 March 1973)

The electronic absorption spectra of $\text{U}(\text{BH}_4)_4$ as a guest in $\text{Hf}(\text{BH}_4)_4$ host crystals are reported. Optical spectra, from the charge transfer or f -to- d cutoff at approximately 2900 Å to the low energy limit due to host molecular vibrations at approximately 2.0 μm, have been obtained at 300, 77, and 2°K for mixed crystals of $\text{U}(\text{BH}_4)_4/\text{Hf}(\text{BH}_4)_4$ and $\text{U}(\text{BD}_4)_4/\text{Hf}(\text{BD}_4)_4$. From temperature effects, deuteration shifts, and intensity patterns, over 20 possible forced electric dipole crystal field electronic origins have been identified. Several molecular vibrations have been identified built on these origins and, based on physically reasonable arguments, are tentatively associated with specific vibrational symmetries and motions of $\text{M}(\text{BH}_4)_4$ type molecules. Attempts to obtain EPR spectra between 2 and 77°K are discussed. Zeeman spectra in fields of up to 93.5 kG for the region 4000–7500 Å have been used to aid in the identification of both ground and excited electronic crystal field states. Calculations, based on a free ion and cubic crystal field parameterized Hamiltonian, are employed to assign electronic origins. The spectra are best fit to a crystal field model Hamiltonian whose two parameters $A_{60} \langle r^6 \rangle$ and $A_{40} \langle r^4 \rangle$ have their signs determined from considerations of 12 negative point charges at the hydrogen positions. Implications of these crystal field and vibrational analyses for actinide spectroscopy are discussed.

I. INTRODUCTION

While electronic states of molecular crystals have been studied for quite some time, almost all theoretical and experimental investigations have been confined to aromatic organic crystals. In order to broaden the base upon which understanding of molecular solids rests, an investigation of inorganic molecular crystals has been initiated. One main goal of this research is to determine if concepts developed over the years for description of organic systems¹ are equally applicable to the uninvestigated class of inorganic molecular systems.

As part of this study, which also includes transition metal hexafluorides and hexachlorides, several synthetic and spectroscopic investigations of rare earth and actinide borohydrides^{2,3} have been started. This first paper will deal with visible and near infrared electronic absorption and Zeeman spectra of uranium borohydride, $\text{U}(\text{BH}_4)_4$, and its deuterated analogue $\text{U}(\text{BD}_4)_4$ in mixed crystals of hafnium (zirconium) borohydride, $\text{Hf}(\text{BH}_4)_4$, and hafnium borodeuteride, $\text{Hf}(\text{BD}_4)_4$. Uranium borohydride is, in many ways, exemplary of inorganic molecular crystal systems: it has a large number of different, accessible electronic states; it has high symmetry, preserved in some crystal environments, so it is possible to detail effects of vibronic coupling and various external perturbations on degenerate electronic states; it presents geometry, crystal structure, and types of atoms different from the more heavily investigated organic systems.

The mixed crystal hosts hafnium and zirconium borohydrides were chosen for the initial study of spectroscopic properties of $\text{U}(\text{BH}_4)_4$ because of their high site symmetry at low temperatures, simple crystallographic structure, and the substitutional nature (*vide infra*) of the $\text{U}(\text{BH}_4)_4/\text{Hf}$, $\text{Zr}(\text{BH}_4)_4$ mixed crystal. These mixed crystals, as well as $\text{U}(\text{BH}_4)_4/\text{Th}(\text{BH}_4)_4$, have all the advantages of isotopic mixed crystals in terms of substitutional structure plus the advantages of very deep trap chemical mixed crystals. That is to say, the *ideal mixed crystal* limit⁴ is realized for these systems because the hosts have no nonbonded electrons. The first host electronic transitions usually occur above 40 000 cm^{-1} while typical d - d or f - f transitions for inorganic molecules of interest are usually below 25 000 cm^{-1} and extend well into the near infrared. Of course, it must be remembered that these are still "chemical mixed crystals" and structural differences, even though the various molecules can go from one lattice to another substitutionally, may occur. In fact, such a situation obtains for the hafnium-zirconium-thorium-uranium borohydride crystal systems, as is discussed in Sec. II. It is then quite informative to compare pure crystal exciton states to the associated ideal mixed crystal energy levels in both substitutional mixed crystals. Pure crystal spectra have been obtained and are currently being analyzed.⁴

From a chemical standpoint, $\text{U}(\text{BH}_4)_4$ offers the possibility of using the $(5f)^2$ electrons of U^{4+} as optical and magnetic probes of the nature of metal-borohydride bonding and fluxionality.² Only after a

thorough understanding of the energy levels of the molecule has been achieved, however, can this probe be utilized. In this paper we present necessary developmental work for both molecular crystal and bonding studies.

The more immediate significance of $U(BH_4)_4$ optical and Zeeman spectra presented here relates to crystal field models as applied to actinide spectra. In the mixed crystal $U(BH_4)_4/Hf(BH_4)_4$, $U(BH_4)_4$ occupies a full tetrahedral (T_d) symmetry site (see Sec. II). As a consequence of this high site symmetry, there are comparatively few, intense electronic ($f-f$) transitions. Absence of the $\bar{1}$ operation in the site group allows forced electric dipole intensity at electronic origins. Observation and assignment of electronic crystal field transitions are thereby made relatively more simple than for other actinide crystal spectra. Being the most volatile U^{4+} compound known, $U(BH_4)_4$ should provide a test of expected effects of covalency on conventional parameterizations of actinide spectra. These effects should be recognizable as a decrease in free ion parameters⁵ and possibly even breakdown of the crystal field model itself.

II. CRYSTAL STRUCTURE OF $Hf(BH_4)_4$, $Zr(BH_4)_4$, $U(BH_4)_4$ AND $Th(BH_4)_4$

The crystal structures of hafnium and zirconium borohydrides are isomorphous and have been determined by both x-ray and neutron diffraction to be $P\bar{4}3m$ with one molecule per unit cell at sites of T_d symmetry.⁶ The structure is cubic even at 24 °K ($a_0 = 5.82 \text{ \AA}$). The molecule therefore has the same structure in gas^{6b} and crystal phases. A picture of the site geometry as determined by neutron diffraction is given in Fig. 1. $U(BH_4)_4$ apparently goes substitutionally into this lattice for a $Hf(BH_4)_4$ or $Zr(BH_4)_4$ molecule and retains this

T_d site symmetry even at 2 °K. There is no spectroscopic or physical evidence to indicate otherwise (*vide infra*).

On the other hand, $U(BH_4)_4$ and $Th(BH_4)_4$ ^{7a} (and presumably $Np(BH_4)_4$, as well) have a different crystal structure. The tetragonal space group, determined by x-ray^{7b} and neutron diffraction,^{7c} is $P4_12_12$ ($P4_32_12$), with four molecules per unit cell at equivalent sites of C_2 symmetry. Here the molecular structure is quite different, and uranium atoms are now surrounded by 14 rather than 12 hydrogen atoms. Discussion of this structure change can be found in Ref. 7(c).

III. EXPERIMENTAL

Syntheses and purification of all compounds used were carried out in grease-free vacuum systems whose working pressures were in the range of 10^{-6} – 10^{-7} torr. $Hf(BH_4)_4$ was made by the solvent-free reaction of $HfCl_4$ (Research Inorganic) and $LiBH_4$ (Alpha)⁸; $U(BH_4)_4$ was made by reaction of UF_4 (Research Inorganic) with $Al(BH_4)_3$ ⁹; and $Al(BH_4)_3$ was made by reaction of $AlCl_3$ (Rocky Mountain Research) with $LiBH_4$.¹⁰ All deuterides were made similarly by employing $LiBD_4$ of greater than 95% isotopic purity, (International Chemical and Nuclear), as the deuterium source. Synthesized compounds were purified by repeated vacuum sublimations. Samples were stored in well degassed glass ampoules fitted with breakseals and were sublimed immediately before use.

Mixed crystals of $U(BH_4)_4$ in $Hf(BH_4)_4$ and of $U(BD_4)_4$ in $Hf(BD_4)_4$ were vapor grown. The desired amounts of host and guest were first sublimed into a quartz cell and subsequently sealed off under vacuum. The host was then melted ($\sim 35 \text{ }^\circ\text{C}$) and a solution was formed. This mixture was frozen ($\sim 0 \text{ }^\circ\text{C}$) in either a side arm of the cell or in the

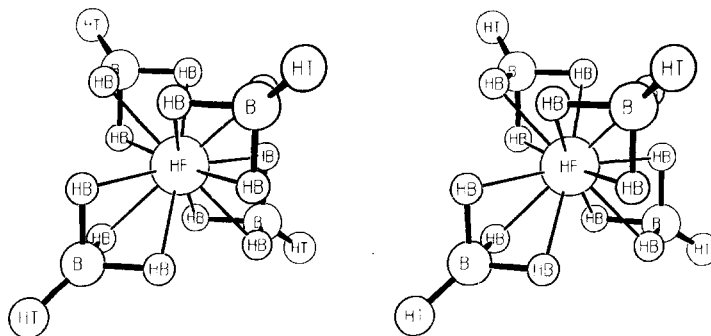


FIG. 1. Stereoscopic representation of the $Hf(BH_4)_4$ site geometry. All atoms are represented by arbitrarily sized spheres at positions determined by neutron diffraction. HB is the bridging hydrogen, and HT is the terminal hydrogen. HF sits at (000) in $P\bar{4}3m$, 1 molecule/unit cell. This drawing is representative of the $U(BH_4)_4$ molecular structure in gas, solution, and $Hf(BH_4)_4$ mixed crystal phases.

end of the cell opposite the optical path. When the solid solution came to room temperature, the optical tip of the cell was cooled by contact with a copper wire dipped in an ice water bath. Crystals of up to 20 mm path length can be grown this way in 2–10 days, with as much as 1.0 mole% of $U(BH_4)_4$. Spectroscopic samples for use in low temperature studies were lowered into liquid nitrogen over a 2–4 day period in order to minimize cracking.

Optical absorption cells were constructed of two Pyrex breakseals and a commercial quartz lower section which formed the optical path. Short (1–5 mm) optical paths were made by flattening quartz tubing; longer paths were obtained by using square or rectangular quartz tubing. The region between breakseals was evacuated, degassed, filled with about 700 mm Hg of helium gas and sealed off. Before spectra were taken on such a sample, the breakseal between the stored helium gas and the crystal was opened. The resultant pressure over the sample at 300 °K was roughly 300 mm Hg and provided some thermal contact between crystal and coolant bath. All data were taken with cells bathed in the cryogen; spectra gave no indication that sample crystals were significantly warmer than the coolant bath. Glass and stainless steel Dewars used were equipped with Suprasil windows. Low temperature optical data were taken at 2, 4, 2, and 77 °K.

Electronic absorption spectra of mixed crystals at 77 and 2 °K were taken on a Cary 14R in the wave length region 3000–25 000 Å and were referenced to air. Spectra of undoped host crystals of equal path length were similarly recorded to determine absorptions due to host vibrational overtones or to quartz. Typical resolution in the region 3500–6500 Å was 1–2 Å while in the near infrared, 6500–20 000 Å, resolution was ~7 Å. Accuracy of peak positions is, of course, a function of their shape and intensity; strong, sharp peaks were measured to ± 1.0 Å, broad weak ones were sometimes no better measured than ± 20 Å. Peak energy errors are based on measurements of several tracings of the same absorption maxima.

The photographic region (3000–9000 Å) of this spectrum was also observed on a 2 m spectrograph capable of a first order resolution of 0.1 Å. No additional structure was found. Frequencies measured relative to a superimposed iron hollow-cathode standard matched those obtained from Cary spectra to within available accuracy. Spectra presented in this paper were all taken on a Cary 14R.

Gas phase spectra were photographically recorded using a 2 m White-type multipass sample cell.¹¹ Visible absorption spectra were taken at

300 °K ($P \sim 0.1$ torr) with a 72 m effective path length. From 2000 to 3000 Å a 10 cm cell at 0.1 torr pressure was adequate to record good spectra.

Sample cells for paramagnetic resonance studies (EPR) were 25 cm long, 3.0 mm o. d. thin wall suprasil quartz tubes. Mixed crystal samples, which occupied the lower 3 cm of this tube, were grown as described above and sealed off under vacuum. Paramagnetic resonance spectra were sought with a Varian E-15 and a Varian E-12 spectrometer operating at a nominal frequency of 9.0 GHz.¹² Samples were again immersed in boiling helium; the Dewar had an 11 mm o. d. tail section which fit into a standard Varian X-band cavity. This tail section contained both sample tube and boiling helium and probably maintained sample temperature somewhat above 4.2 °K. Some experiments were done with an Air Products Cryo-tip EPR accessory attached to the Varian cavity.¹² This allowed sample temperatures of ~6 °K and higher to be obtained. Experiments at 77 °K were also run in a similar Dewar containing liquid N_2 .

Zeeman effect data were obtained for $U(BD_4)_4$ in $Hf(BD_4)_4$ at the MIT National Magnet Laboratory. Spectra were recorded on photographic plates with a Bausch and Lomb 2 m spectrograph, capable of 0.1 Å resolution in first order. Various fields up to 93.5 kG were used with H perpendicular to the direction of light propagation.

IV. GENERAL SPECTROSCOPIC RESULTS

Perhaps the most striking feature of uranium borohydride is its color in various environments. Pure crystals and ether solutions are dark green while $Hf(BH_4)_4$ mixed crystals and hydrocarbon solutions are pink. This is, of course, due to structure changes from monomeric T_d symmetry molecules in the latter forms to "polymeric" C_2 symmetry species in pure crystals. [Unlike lanthanide (4f) compounds, ligand symmetry changes can drastically alter spectra of actinides due to the much larger crystal fields in 5f systems.] As expected, pure crystals of $U(BH_4)_4$ evidence polarized absorption spectra.

At room temperature, spectra of $U(BH_4)_4$ in hydrocarbon solutions, $Hf(BH_4)_4$ solutions, and mixed crystals consist of several broad bands. Absorption in these three systems are identical over the range studied (3000–9000 Å). The gas phase spectrum has the same appearance as the above "dilute solvent" spectra, but the bands are shifted to the blue by between 100 and 300 cm^{-1} . In vapor, solution, and mixed crystal the intense charge transfer and/or $f-d$ transition cutoff commences at 2900 Å (this cutoff begins at 4100 Å in pure crystal). Spectra of the borohydride and borodeuteride are quite

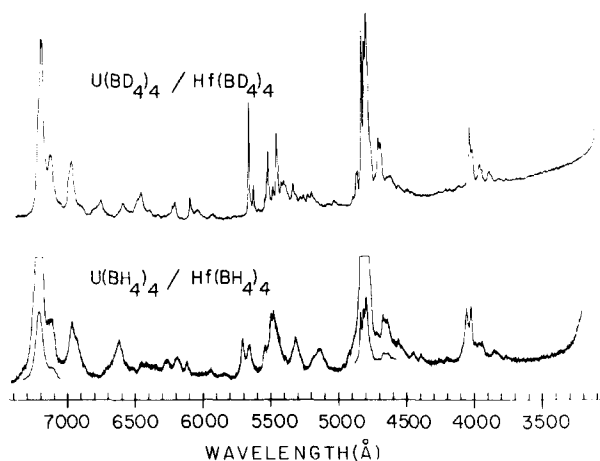


FIG. 2. Absorption spectra of $U(BD_4)_4/Hf(BD_4)_4$ (top) and $U(BH_4)_4/Hf(BH_4)_4$ (bottom) from 3000 to 7000 Å at 2 °K. Horizontal scale is wavelength in angstroms; vertical is arbitrary absorbance. Increase in intensity at ~ 3300 Å is the start of the charge transfer cutoff; 7000 Å region is repeated in Fig. 3 at a lower dispersion.

similar at room temperature.

At lower temperatures, mixed crystal spectra sharpen and show considerable structure as can be seen in Figs. 2 and 3. All spectroscopic results are consistent with T_d symmetry for $U(BH_4)_4$ substituted in $Hf(BH_4)_4$ to 2 °K. It can therefore be concluded that there is no phase transformation to lower than T_d symmetry between 24 and 2 °K for $Hf(BH_4)_4$ or $Zr(BH_4)_4$. On cooling from 77 to 2 °K there is a further sharpening of absorption features and a detectable shift in energy for some peaks. It is important to note that no hot bands have been found as crystals are warmed from 2 to 77 °K. This is consistent with there being no excited electronic states of energy less than 100 cm^{-1} and greater than about 10 cm^{-1} . No differences between $U(BH_4)_4/Hf(BH_4)_4$ and $U(BH_4)_4/Zr(BH_4)_4$ mixed crys-

tal spectra have been detected in any experiments. Also, no differences have been noted between 4.2 and 2 °K; hence all optical data presented are for 2 °K.

The low temperature spectra do, however, undergo considerable change upon sample deuteration. As shown in Fig. 2, the visible spectrum of the deuteride is much sharper than that of the hydride, and there are also shifts in energy of many of the prominent features. These shifts upon deuteration can be characterized in three ways: blue shifts due to increased field and/or zero point effects in the deuteride; red shifts for electronic states for which transition energy decreases with increasing crystal field strength; and relative shifts for groups of peaks whose energy separations decrease upon deuteration due to an isotopic effect on vibrational spacings. If borohydride and borodeuteride spectra are taken together, interpretation of $U(BH_4)_4$ electronic spectrum becomes obvious. The observed absorption features from 4000 to 20 000 Å can be associated with transitions from a ground electronic state to excited electronic and vibronic states of the uranium borohydride molecule. In addition to their usefulness in electronic origin and molecular vibration identification, the deuteride spectra almost completely remove interference of host vibrational overlap with the low energy end of the electronic spectrum (Fig. 3). It has thus been possible to explore the low energy end of the $U(BD_4)_4$ spectrum to roughly 4000 cm^{-1} . The lowest electronic feature of this system has been identified at 5932 cm^{-1} and only absorptions due to $Hf(BD_4)_4$ have been detected at lower energy. All of the above points can be seen most clearly if individual areas of the spectra of $U(BD_4)_4/Hf(BD_4)_4$ are presented at higher dispersion. In Figs. 4–8 are shown the regions of the $U(BD_4)_4/Hf(BD_4)_4$ mixed crystal spectra which best display this molecular electronic origin plus vibrational structure nature

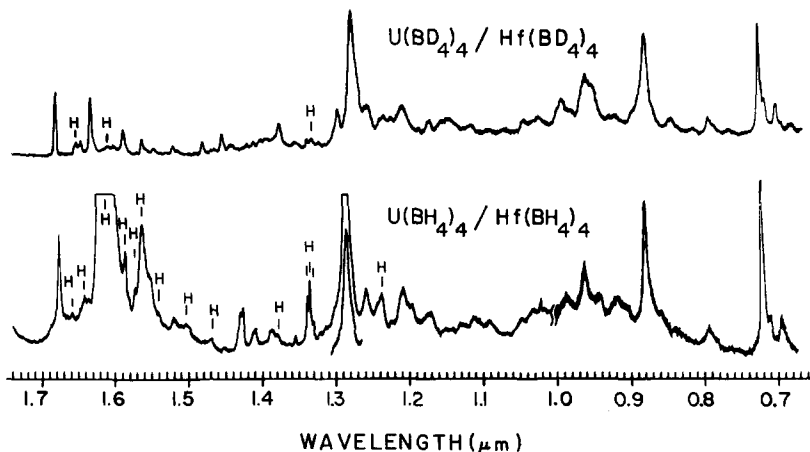


FIG. 3. Absorption spectra of $U(BD_4)_4/Hf(BD_4)_4$ (top) and $U(BH_4)_4/Hf(BH_4)_4$ (bottom) from 0.7 to 1.7 μm at 2 °K. Horizontal scale is wavelength in micrometers, and vertical scale is arbitrary absorbance. All observed absorption beyond 1.7 μm is attributable to the host crystals as are all bands marked H; 0.7 μm region is repeated in Fig. 2 at higher dispersion.

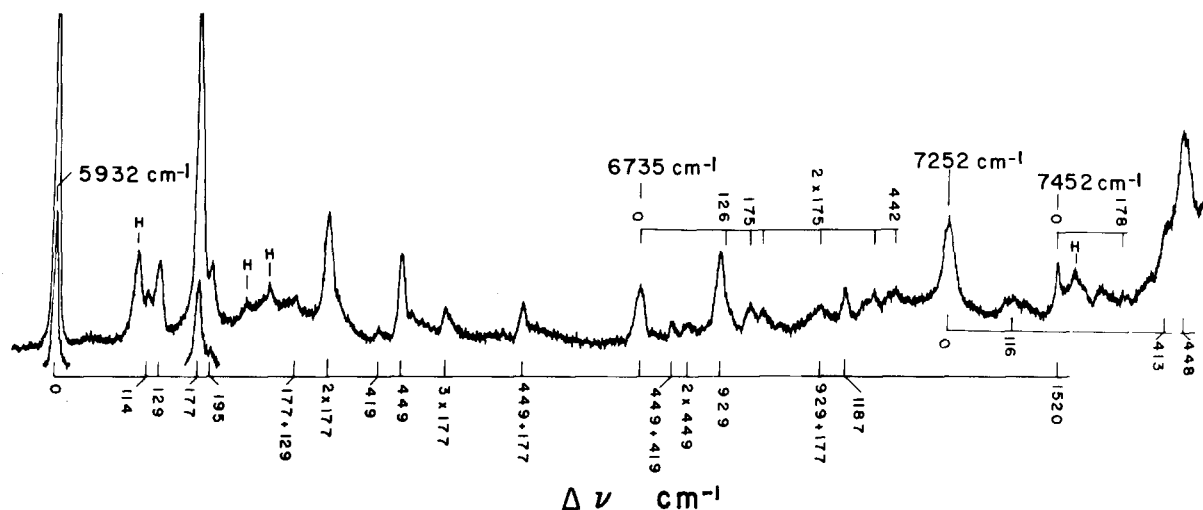


FIG. 4. Higher dispersion absorption spectrum of $U(BD_4)_4/Hf(BD_4)_4$ at 2°K from 1.7 to 1.2 μm . Origins and differences (in cm^{-1}) correlate to the assignments in Table II. H indicates vibration features due to the host crystal. The origin at 5932 cm^{-1} is the lowest observed and corresponds to $T_1(a^3H_5)$ in both models.

of the over-all spectra. The reappearance of certain energy spacings throughout (120, 170, 450 cm^{-1} , etc.) makes this vibrational interpretation even more obvious.

EPR spectra for $U(BH_4)_4$ in $Hf(Zr)(BH_4)_4$ and $U(BD_4)_4$ in $Hf(BD_4)_4$ at both 77 and 4°K failed to give any reproducible, positive results. The region about $g \sim 2.0$, the expected g value for a $T_2(^3H_4)$ ground state, was extensively searched (see Sec. VII) at high and low microwave powers and at temperatures between 4 and 30°K. No structure clearly associated with $U(BH_4)_4$ was found. Magnetic fields up to 12 000 G with X-band radiation were also used to look for low g -value states [$T_1(^3H_4)$]; again a negative result was obtained at 4 and 77°K.

Zeeman effect results show no splitting of any of

the absorption maxima in the 4000–7500 Å region. Furthermore, to the available accuracy (± 2 cm^{-1}), no energy shifts have been observed at fields up to 93.5 kG for the sharpest peaks in this region (16 357, 17 622, and 20 694 cm^{-1}). These features do exhibit a small decrease in peak intensity and presumably some slight broadening at high field values; the largest effect is found on the 16 357 cm^{-1} absorption which evidences a 30% intensity reduction and a 10% broadening at 93.5 kG. In general, however, the visible spectrum of $U(BD_4)_4$ in $Hf(BD_4)_4$ at 93.5 kG is qualitatively identical to that at zero magnetic field.

These seemingly negative EPR and Zeeman results are emphasized here because they will be

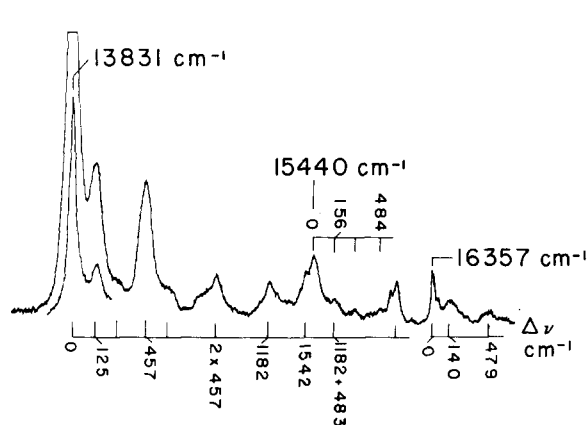


FIG. 5. Higher dispersion absorption spectrum of $U(BD_4)_4/Hf(BD_4)_4$ at 2°K from 7300 to 6000 Å. Origins and differences (in cm^{-1}) correlate to the assignments in Table II.

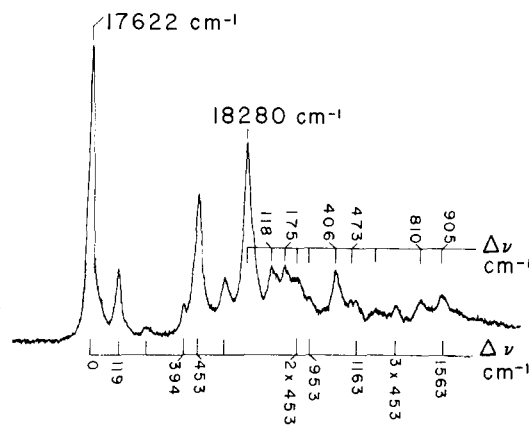


FIG. 6. Higher dispersion absorption spectrum of $U(BD_4)_4/Hf(BD_4)_4$ at 2°K from 5700 to 5100 Å. Origins and differences (in cm^{-1}) correlate to the assignments in Table II.

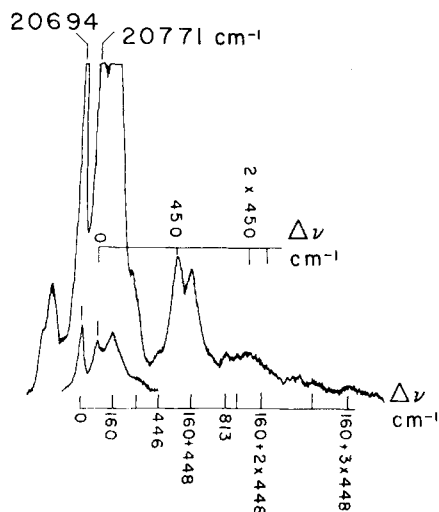


FIG. 7. Higher dispersion absorption spectrum of $U(BD_4)_4/Hf(BD_4)_4$ at 2 °K from 4900 to 4400 Å. Origins and differences correlate to the assignments in Table II. The possible origin cc is indicated here as 160 built on 20 694 cm^{-1} . Vibrations built on cc are indicated as added to 20 694 + 160.

shown to be central to an understanding of the energy level structure and optical absorption spectra of $U(BH_4)_4$.

V. DETERMINATION OF ELECTRONIC ORIGINS AND MOLECULAR VIBRATIONS

The lowest energy electronic configuration of U^{4+} is $(5f)^2$ outside the closed shell rare gas configuration of Rn. From consideration of allowed Russell–Saunders terms in $(5f)^2$, it follows that there are 40 energy levels for U^{4+} in a cubic crystal site; $7A_1 + 3A_2 + 9E + 9T_1 + 12T_2$. For a T_d site symmetry both magnetic and (forced) electric dipole ($E1$) transitions are allowed for pure electronic origins and Table I contains a listing of possible transitions for different symmetry ground states. Well over 200 transitions have been found between 5000 and 30 000 cm^{-1} (see Figs. 2 and 3); therefore, simple numerics dictate that the absorption spectra be assigned on the basis of electronic origins and molecular vibrations built on them. Lattice modes of this 1 molecule/unit-cell molecular crystal can be excluded as contributing to the spectrum based on energy considerations, Franck–Condon arguments, and number of observed features.

Progressions of some few frequencies built upon several origins and reappearance of several other frequency differences are quite obvious in a closer inspection of the absorption spectra. Intensity patterns of progressions generally follow the simple Franck–Condon envelope expected for only

small displacements of equilibrium geometry upon electronic excitation. These points are well illustrated in $U(BD_4)_4/Hf(BD_4)_4$ spectra at higher dispersion presented in Figs. 4–8. In each figure, probable electronic origins for that spectral region are indicated in wavenumbers above the peak and structure assigned to vibrations built on those origins is similarly indicated. In Table II is presented a tabulation of data for $U(BD_4)_4/Hf(BD_4)_4$ with present vibrational assignments. These regularities taken with above mentioned hydrogen–deuterium and temperature shifts (columns 5 and 6, Table II) make it possible to identify ~30 possible origins ranging from 5932 to 24 795 cm^{-1} in $U(BD_4)_4$. Built on these origins are a number of vibrations, which are presumed to be of the molecule. These frequencies are given in Table III along with vibrational data on $Hf(BH_4)_4$ for comparison. Most prominent features of the hydride spectrum can be simply related to the deuteride origins or vibrations and were similarly assigned. Unfortunately, a complete normal coordinate analysis of $M(BH_4)_4$ type molecules is not available. Such a study has been initiated,¹³ but, for the moment, reasonability arguments must be relied upon for vibrational assignments.

Vibrational spectra of vapor phase $U(BH_4)_4$ have recently been published¹⁴ and have been interpreted in terms of a structure identical to that of $Hf(BH_4)_4$ and $Zr(BH_4)_4$. These results are totally consistent with data presented here. Comparison of vibrations determined from the electronic spectra with known infrared and Raman data on Hf, Zr(BH_4)₄ and Hf, Zr(BD_4)₄^{13,15,16} points to their reasonability (Table III).

For a T_d $M(BH_4)_4$ molecule, $4A_1 + A_2 + 5E + 5T_1 + 9T_2$ vibrational modes are expected. Raman polarization data singles out the A_1 modes as 552(521), 1290(960), 2195(1562), and 2570(1929) cm^{-1} for $Hf(BH_4)_4[Hf(BD_4)_4]$, as given in Table III.

TABLE I. Electronic transition selection rules for U^{4+} , $(5f)^2$, in a T_d site.

Ground state	$E1$ allowed ^a excited states	$M1$ allowed ^b excited states
A_1	T_2 (10)	T_1 (8)
A_2	T_1 (8)	T_2 (10)
E	T_1, T_2 (18)	T_1, T_2 (0)
T_1	A_2, E, T_1, T_2 (28)	A_1, E, T_1, T_2 (5)
T_2	A_1, E, T_1, T_2 (30)	A_2, E, T_1, T_2 (3)

^aNumber in parentheses is the number of forced electric dipole origins expected in the 5000–30 000 cm^{-1} region for the $H(12)$ model.

^bNumber in parentheses is the number of magnetic dipole origins that are *not* electric dipole allowed in the 5000–30 000 cm^{-1} region.

TABLE II. Absorption spectrum of $U(BD_3)_4/Hf(BD_3)_4$ at 2°K; summary of electronic transitions and vibrational assignments.

Wave length in Air ^a (Å)	Error ^b (± Å)	Vacuum corrected energy (cm ⁻¹)	Relative intensity	H → D ^c shift (cm ⁻¹)	77 → 2°K ^d shift (cm ⁻¹)	Assignment ^e to origins and $\Delta\nu$ (cm ⁻¹)	Vibrational ^f identification
16 852	4	5 932	95	-27	-7	<i>origin a</i>	
16 536	3	6 046	5			<i>a</i> +114	<i>a</i> + ν_α
16 495	3	6 061	15			<i>a</i> +129	<i>a</i> + ν_β
16 365	4	6 109	75			<i>a</i> +177	<i>a</i> + ν_δ
16 318	4	6 127	5			<i>a</i> +195	(<i>a</i> + ν_ϵ)
16 029	(3)	6 237	5			<i>a</i> +305	<i>a</i> + ν_δ + ν_β
15 919	3	6 280	25			<i>a</i> +348	<i>a</i> +2 ν_δ
15 741	[5]	6 351	2			<i>a</i> +419	(<i>a</i> + ν_ζ)
15 667	3	6 381	18			<i>a</i> +449	<i>a</i> + ν_η
15 630	[10]	6 396	3			<i>a</i> +464	<i>a</i> +2 ν_δ + ν_α
15 514	3	6 444	6			<i>a</i> +512	<i>a</i> +3 ν_δ
15 246	3	6 557	7			<i>a</i> +625	<i>a</i> + ν_η + ν_δ
15 198	(4)	6 578	2			<i>a</i> +646	(<i>a</i> + ν_η + ν_ϵ)
14 844	3	6 735	11	...	-10	<i>origin b</i>	
14 735	(3)	6 785	2			<i>a</i> +853	(<i>a</i> + ν_η + ν_ζ)
14 681	(3)	6 810	2			<i>a</i> +878	(<i>a</i> +2 ν_η)
14 572	3	6 861	12			<i>a</i> +929	<i>a</i> + ν_λ (<i>a</i> + ν_η + ν_θ)
14 467	3	6 910	6			<i>b</i> +175	<i>b</i> + ν_δ
14 422	(3)	6 932	3			<i>b</i> +197	(<i>b</i> + ν_ϵ)
14 360	(5)	6 962	1			<i>a</i> +1030 <i>b</i> +227	
14 225	(4)	7 028	3			<i>b</i> +293	(<i>b</i> + ν_β + ν_δ)
14 140	(4)	7 070	7			<i>b</i> +335	<i>b</i> +2 ν_δ
14 044	(4)	7 119	3			<i>a</i> +1187	(<i>a</i> + ν_μ)
13 973	(6)	7 155	2			<i>b</i> +420	(<i>b</i> + ν_ζ)
13 929	(8)	7 177	2			<i>b</i> +442	<i>b</i> + ν_η
13 786	(3)	7 252	19	+47	(+13)	<i>origin c</i>	
13 569	(5)	7 368	4			<i>c</i> +116	<i>c</i> + ν_α
13 415	3	7 452	7	(+73)	-11	<i>a</i> +1520	<i>a</i> + ν_ζ
13 262	(4)	7 538	4			(<i>origin d</i>) <i>a</i> +1606 <i>b</i> +803	
13 181	(8)	7 585	2			<i>a</i> +1653	
13 101	(6)	7 631	2			<i>a</i> +1698	<i>a</i> + ν_ζ + ν_δ
13 043	6	7 665	3			<i>d</i> +178	<i>d</i> + ν_δ
12 986	3	7 698	22			<i>c</i> +413	(<i>c</i> + ν_ζ)
12 803	[5]	7 809	90	+46	+9	<i>c</i> +448	<i>c</i> + ν_η
12 609	(10)	7 929	8			<i>origin e</i>	
12 572	10	7 952	15			<i>e</i> +120	<i>e</i> +(ν_α , ν_β)
12 406	8	8 058	5			<i>e</i> +143	(<i>e</i> + ν_γ)
12 346	4	8 098	12			<i>e</i> +250	<i>e</i> +2(ν_α , ν_β)
12 253	4	8 159	10			<i>e</i> +290	(<i>e</i> +2 ν_γ)
12 097	4	8 264	23			<i>e</i> +350	(<i>e</i> +2 ν_δ)
11 722	(8)	8 529	7	(-11)	(-8)	<i>e</i> +455	<i>e</i> + ν_η
11 534	(10)	8 668	5			<i>e</i> +720	
11 458	(12)	8 725	10			(<i>origin f</i>) <i>e</i> +859	(<i>e</i> + ν_κ)
11 148	6	8 968	5			<i>f</i> +138	(<i>f</i> + ν_γ)
10 928	(25)	9 148	1			<i>e</i> +916	<i>e</i> +2 ν_η <i>e</i> + ν_λ
10 690	(15)	9 352	2			<i>e</i> +1157	(<i>e</i> + ν_μ)
10 426	8	9 589	10	+37	(-4)	<i>f</i> +439	<i>f</i> + ν_η
10 296	18	9 710	3			<i>e</i> +1337	(<i>e</i> + ν_μ + ν_δ)
						<i>f</i> +619	<i>f</i> + ν_δ + ν_η
						<i>e</i> +1543	<i>e</i> + ν_ζ
						<i>origin g</i>	
						<i>g</i> +121	<i>g</i> +(ν_α , ν_β)

TABLE II. *Continued*

Wave length in Air ^a (Å)	Error ^b (± Å)	Vacuum corrected energy (cm ⁻¹)	Relative intensity	H → D ^c shift (cm ⁻¹)	77 → 2° K ^d shift (cm ⁻¹)	Assignment ^e to origins and Δν (cm ⁻¹)	Vibrational ^f identification
10 215	5	9 787	14	(-5)	••	<i>g</i> +198 (<i>origin h</i>)	(<i>g</i> +ν _ε)
9 978	(6)	10 019	4			<i>g</i> +430	<i>g</i> +ν _η
9 918	6	10 080	30	-40	(-5)	<i>g</i> +491 <i>origin i</i>	<i>g</i> +ν _θ
9 792	12	10 210	2			<i>h</i> +423 <i>i</i> +130	<i>i</i> +ν _β
9 655	5	10 354	3			<i>i</i> +274	(<i>i</i> +2ν _β)
9 598	3	10 416	45	+38	-15	<i>origin j</i>	
9 530	(9)	10 490	10			<i>g</i> +901 <i>i</i> +410	(<i>g</i> +2ν _η) (<i>i</i> +ν _ε)
9 497	6	10 527	20			<i>i</i> +447 <i>j</i> +111	<i>i</i> +ν _η <i>j</i> +ν _α
9 225	[10]	10 837	5			<i>j</i> +421	(<i>j</i> +ν _ε)
9 174	(6)	10 897	8			<i>i</i> +817 <i>j</i> +480	(<i>i</i> +ν _κ) <i>j</i> +ν _θ
8 955	(10)	11 164	3			<i>i</i> +1575	(<i>i</i> +ν _ε)
8 778	3	11 389	80	+34	+9	<i>origin k</i>	
8 665	(13)	11 538	5			<i>k</i> +149	(<i>k</i> +ν _γ)
8 425	3	11 866	9			<i>k</i> +477	<i>k</i> +ν _θ
8 107	4	12 322	2			<i>k</i> +953	<i>k</i> +2ν _θ
7 917	3	12 628	13	+56	-20	<i>origin l</i>	
7 847	(10)	12 740	3			<i>l</i> +112	<i>l</i> +ν _α
7 638	(5)	13 089	3			<i>l</i> +461	<i>l</i> +ν _η
7 556	(6)	13 231	2	-12	(-3)	<i>l</i> +603 (<i>origin m</i>)	(<i>l</i> +ν _η +ν _δ)
7 228	[2]	13 831	100	-6	(-4)	<i>origin n</i>	
7 152	3	13 978	20			<i>n</i> +124	<i>n</i> +(ν _α , ν _β)
7 080	[5]	14 120	2			<i>n</i> +268	(<i>n</i> +2(ν _α , ν _β))
6 997	2	14 288	25			<i>n</i> +457	<i>n</i> +ν _η
6 920	6	14 447	3			<i>n</i> +616	(<i>n</i> +ν _η +ν _γ)
6 779	(4)	14 747	7			<i>n</i> +916	<i>n</i> +2ν _η
6 615	(2)	15 113	6	+18	(-2)	<i>n</i> +1182 (<i>origin o</i>)	(<i>n</i> +ν _μ)
6 503	4	15 373	3			<i>n</i> +1542	<i>n</i> +ν _ε
6 475	2	15 440	11	(-40)	(+3)	<i>n</i> +1609 (<i>origin p</i>)	
6 410	5	15 596	2			<i>o</i> +483 <i>p</i> +156	<i>o</i> +ν _θ (<i>p</i> +ν _γ)
6 348	(5)	15 749	2			<i>p</i> +309	(<i>p</i> +2ν _γ)
6 278	(6)	15 924	1			<i>p</i> +484	<i>p</i> +ν _θ
6 244	1	16 011	4	(-124 or +66)	(+8)	<i>o</i> +897 (<i>origin q</i>)	(<i>o</i> +2ν _η)
6 226	1	16 057	9	(-78 or +112)	+13	<i>o</i> +944 (<i>origin r</i>)	(<i>o</i> +ν _λ)
6 178	(4)	16 182	1			<i>q</i> +171 <i>r</i> +126	<i>q</i> +ν _δ <i>r</i> +ν _β
6 112	2	16 357	10	+32	+11	<i>origin s</i>	
6 098	[5]	16 394	2			<i>q</i> +383	<i>q</i> +ν _θ
6 060	(6)	16 497	3			<i>q</i> +486 <i>s</i> +140	(<i>s</i> +ν _γ) <i>s</i> +ν _θ
5 938	(8)	16 836	2			<i>s</i> +479	<i>s</i> +ν _θ
5 890	[10]	16 973	1			<i>p</i> +1533	(<i>p</i> +ν _ε)
5 790	[8]	17 266	1			<i>s</i> +909	(<i>s</i> +ν _λ)
5 673	1	17 622	62	+120	+19	<i>origin t</i>	
5 657	[3]	17 672	1			<i>t</i> +50	
5 635	1	17 741	13			<i>t</i> +119	<i>t</i> +ν _α
5 598	(2)	17 859	1			<i>t</i> +237	<i>t</i> +2ν _α

TABLE II. *Continued*

Wave length in Air ^a (Å)	Error ^b (± Å)	Vacuum corrected energy (cm ⁻¹)	Relative intensity	H → D ^c shift (cm ⁻¹)	77 → 2° K ^d shift (cm ⁻¹)	Assignment ^e to origins and Δν (cm ⁻¹)	Vibrational ^f identification
5549	1	18 016	3			<i>t</i> + 394	(<i>t</i> + ν _ε)
5531	1	18 075	26			<i>t</i> + 453	<i>t</i> + ν _η
5494	2	18 197	7			<i>t</i> + 575	<i>t</i> + ν _η + ν _α
5469	1	18 280	35	+44	+8	<i>origin u</i>	
5434	1	18 398	6			<i>u</i> + 118	<i>u</i> + ν _α
5417	1	18 455	6			<i>u</i> + 175	<i>u</i> + ν _δ
5399	2	18 517	3			<i>t</i> + 895	(<i>t</i> + 2ν _η)
						<i>u</i> + 237	<i>u</i> + 2ν _α
5382	2	18 575	2			<i>t</i> + 953	(<i>t</i> + ν _λ)
						<i>u</i> + 295	<i>u</i> + ν _δ + ν _α
5350	2	18 686	10			<i>u</i> + 406	(<i>u</i> + ν _ε)
5331	(4)	18 753	1			<i>u</i> + 473	<i>u</i> + ν _θ
5322	3	18 785	3	<i>t</i> + 1163	(<i>t</i> + ν _μ)
						(<i>origin v</i>)	
5297	(3)	18 873	2			<i>u</i> + 593	<i>u</i> + ν _θ + ν _α
5270	4	18 970	3			<i>t</i> + 1348	<i>t</i> + 3ν _η
5237	3	19 090	4	...	+11	<i>u</i> + 810	(<i>u</i> + 2ν _ε)
						(<i>origin w</i>)	(<i>v</i> + ν _κ)
5211	2	19 185	4	(-89)	+8	<i>t</i> + 1563	<i>t</i> + ν _ξ
						<i>u</i> + 905	(<i>u</i> + ν _λ)
						(<i>origin x</i>)	
5186	(4)	19 277	1			<i>v</i> + 492	(<i>v</i> + ν _θ)
5160	(4)	19 374	1			<i>x</i> + 192	(<i>x</i> + ν _ε)
5096	(6)	19 618	1			<i>u</i> + 1338	
						<i>x</i> + 433	(<i>x</i> + ν _η)
5040	2	19 836	3	...	+12	<i>u</i> + 1560	<i>v</i> + ν _ξ
						(<i>origin y</i>)	
5024	(6)	19 899	1			<i>u</i> + 1623	
4902	(2)	20 394	2			<i>x</i> + 1209	
						<i>y</i> + 556	
4874	1	20 511	2			<i>x</i> + 1326	
						<i>y</i> + 675	
4867	1	20 541	15	...	(+4)	<i>x</i> + 1356	
						(<i>origin z</i>)	
4831	[2]	20 694	80	+34	+12	<i>origin aa</i>	
4813	[2]	20 771	30	+21	+8	<i>origin bb</i>	
4794	[2]	20 854	75	+18	+16	<i>aa</i> + 160	(<i>aa</i> + ν _δ)
						(<i>origin cc</i>)	
4760	(7)	21 003	4			<i>cc</i> + 149	
						<i>z</i> + 462	<i>z</i> + ν _η
4729	[5]	21 140	1			<i>aa</i> + 446	<i>aa</i> + ν _η
4711	1	21 221	18			<i>bb</i> + 450	<i>bb</i> + ν _η
4694	1	21 298	15			<i>cc</i> + 448	<i>cc</i> + ν _η
4647	(2)	21 513	3			<i>z</i> + 972	
						<i>aa</i> + 819	(<i>aa</i> + ν _κ)
4633	(2)	21 578	1			<i>z</i> + 1037	
						<i>aa</i> + 884	(<i>aa</i> + 2ν _η)
4619	(4)	21 644	3			<i>bb</i> + 869	(<i>bb</i> + 2ν _η)
4593	(6)	21 766	1			<i>cc</i> + 916	(<i>cc</i> + 2ν _η)
4560	(7)	21 924	2			<i>aa</i> + 1230	
						<i>cc</i> + 1070	
4536	(4)	22 040	1			<i>aa</i> + 1346	(<i>aa</i> + 3ν _η)
4498	(3)	22 226	2			<i>aa</i> + 1532	<i>aa</i> + ν _ξ
4259	[5]	23 473	1			<i>aa</i> + 2767	
4206	[5]	23 769	2	(-62)	(-91)	<i>aa</i> + 3075	
						(<i>origin dd</i>)	
4176	[5]	23 940	2			<i>dd</i> + 171	<i>dd</i> + ν _ξ
4112	[5]	24 312	2			<i>dd</i> + 543	
4032	2	24 795	27	+135	(+6)	<i>origin ee</i>	

TABLE II. *Continued*

Wave length in Air ^a (Å)	Error ^b (± Å)	Vacuum corrected energy (cm ⁻¹)	Relative intensity	H - D ^c shift (cm ⁻¹)	77 → 2° K ^d shift (cm ⁻¹)	Assignment ^e to origins and Δν (cm ⁻¹)	Vibrational ^f identification
4 011	2	24 924	10			ee + 129	ee + ν _β
3 956	2	25 271	7			ee + 476	ee + ν _θ
3 937	2	25 393	3			ee + 598	ee + ν _θ + ν _β
3 882	2	25 753	5			ee + 958	ee + (2ν _θ , ν _λ)
3 866	2	25 859	2			ee + 1064	ee + 2ν _θ + ν _β
3 813	(3)	26 219	2			ee + 1424	ee + 3ν _θ
3 791	(6)	26 371	1			ee + 1576	ee + 3ν _θ + ν _β
3 752	[4]	26 645	1			ee + 1850	(ee + 4ν _θ)

^aWavelengths are taken from Cary 14R scans. Presented here are center of peak measurements averaged over several tracings.

^bError is observed range of measurements, peak position plus or minus error indicated. Errors without brackets are based on at least three different samples; arrows in parentheses are based on two samples; and errors in square brackets are based on at least two traces of a thin sample if for a strong intensity peak or are just estimated from traces of the thickest sample if for a weak intensity band.

^cNumbers tabulated are $[\nu(D) - \nu(H)]$ for all features considered to be possible electronic origins. Values in parentheses are based on hydride maxima that are felt to be only tentatively assigned as origins.

^dNumbers tabulated are $[\nu(2^\circ K) - \nu(77^\circ K)]$ for all features considered to be possible electronic origins. Shifts in parentheses are considered to lie within experimental error of being unobserved.

^eAll features considered to be possible origins are indicated by letter. Features not felt to be origins are indicated by an origin and difference in frequency from that origin. Origins considered to be in doubt are in parentheses.

^fVibrational assignments are indicated by origin plus ν_i which corresponds to Column 1 of Table III. Assignments regarded as tentative are in parentheses (see Sec. V).

Three frequency differences are found in the optical spectra that could correspond to the lowest A_1 's in $U(BD_4)_4$: ~ 476 cm⁻¹, ν_θ (Figs. 5 and 8); ~ 930 cm⁻¹, ν_λ (Figs. 4 and 5); and ~ 1530 cm⁻¹, ν_t (Figs. 4 and 6). The 930 cm⁻¹ difference suffers from interference with 2×476 cm⁻¹; but comparison with $U(BH_4)_4$ seems to substantiate its presence. The only other differences which were found to be greater than 500 cm⁻¹ are 812 cm⁻¹, ν_κ (Fig. 4), and 1160 cm⁻¹, ν_μ (Fig. 4). However, these differences have been observed only in regions of low intensity and are thus in doubt. The 1160 cm⁻¹ frequency is probably not a $U(BD_4)_4$ fundamental. The 812 cm⁻¹ difference does correlate well to $Hf(BD_4)_4$ results for a Raman detected, E symmetry vibration but suffers from possible interference with 2×410 cm⁻¹. The highest energy modes are not expected to couple well to U^{4+} $f-f$ transitions as they involve mostly B-D_i motion.

Most differences observed are lower than 500 cm⁻¹ and probably correspond to motions of the whole BD_4 group about the U^{4+} center. In fact, six low energy modes are expected: ($A_1 + T_2$) stretch of the BD_4 to metal bond, $\nu(U-B)$; ($E + T_2$) bends of the BD_4 groups toward each other, $\delta(U-B)$; and the expected low energy torsions ($A_2 + T_1$) of the BD_4 group about the C_3 axes of the molecule, $\tau(BD_4)$. From infrared and Raman data, both $\nu(U-B)$'s and at least one $\delta(U-B)$ have been found

for $Hf(BD_4)_4$: 521 cm⁻¹, $A_1 - \nu(U-B)$; 473 cm⁻¹, $T_2 - \nu(U-B)$; and 211 cm⁻¹, E or $T_2 - \delta(U-B)$. The torsions cannot be directly observed in the ir or Raman, hence we can only conjecture that they are quite low in energy (perhaps < 150 cm⁻¹).

In $U(BD_4)_4$ optical spectra the A_1 and T_2 $\nu(U-B)$ modes apparently occur at ~ 476 cm⁻¹, ν_θ , and 450 cm⁻¹, ν_η , (Figs. 4 and 7) respectively. There is the possibility that these frequencies correspond to the same vibration in various electronic states as they are not observed together built on the same origin; but consistent groupings of the observed differences around 450 and 476 cm⁻¹ argue against

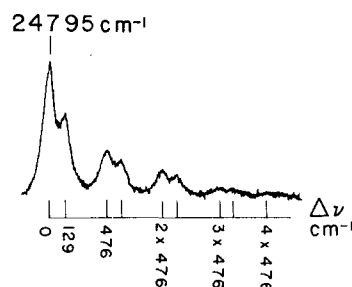


FIG. 8. Higher dispersion absorption spectrum of $U(BD_4)_4/Hf(BD_4)_4$ at 2° K from 4100 to 3600 Å. Origin and differences correspond to the assignments in Table II. This is the highest energy observed origin corresponding to $T_2(^3P_2)$ in both models.

that. E or T_2 , $\delta(U-B)$, may then be assigned to the recurring 176 cm^{-1} , ν_6 (Figs. 4 and 6), difference. It is possible that 195 cm^{-1} , ν_ϵ (Fig. 4), is the other $\delta(U-B)$, but this is not an often seen difference and must be considered to be in doubt. The $140\text{--}150\text{ cm}^{-1}$, ν_γ (Fig. 5), differences only occur in very weak and/or poorly resolved areas and must be considered tentative. The lowest differences, 116 and 129 cm^{-1} , ν_α and ν_β (Figs. 4, 6, and 8), may be only one vibration, but both occur built on the 5932 cm^{-1} origin. Their low energy and closeness suggest an assignment as the A_2 and T_1 , $\tau(BD_4)$; such an assignment is regarded as probable, at least for one of the frequencies. A 410 cm^{-1} ,

ν_ζ (Figs. 4 and 6), difference is also observed; although seemingly too high an energy for a $\delta(U-B)$ and too low an energy for a $\nu(U-B)$, this difference may correspond to either 2×195 , $3 \times 129\text{ cm}^{-1}$, or a fundamental whose energy is not given correctly by this simple model.

To add a note of caution, it should be pointed out that any of these differences, particularly 116 and 129 cm^{-1} , could well correspond to twice a true fundamental frequency. Considering the present state of understanding of $M(BH_4)_4$ vibrations, we cannot eliminate this possibility but note that the above rather naive interpretation of the vibrational

TABLE III. Frequency differences from $U(BD_4)_4/Hf(BD_4)_4$ electronic absorption spectra as compared to ground state vibrational frequencies of $Hf(BD_4)_4$, $Hf(BH_4)_4$, and $U(BH_4)_4$.

U(BD ₄) ₄ /Hf(BD ₄) ₄ frequency difference from electronic spectra		U(BH ₄) ₄ ^d ground state vibrations				Method of detection ^e	Tentative symmetry assignment
Designation ^a	Energy ^b (cm ⁻¹)	Hf(BD ₄) ₄ ^c vibrations (cm ⁻¹)	Hf(BH ₄) ₄ ^c vibrations (cm ⁻¹)	vibrations (cm ⁻¹)			
ν_α	116						
ν_β	129						A_2, T_1
ν_γ	(144)						
ν_δ	176		215		ir		T_2
ν_ϵ	(195)	211	230		R		T_2, E
ν_ζ	(410)						
ν_η	450	473	487	478	ir		T_2
ν_θ	476	521	552		R-p		A_1
		830	1020		ir		$T_2(?)$
ν_κ	(812)	815	1088		R		E
			1140	1110	ir		
		923	1228	1230	ir		T_2
ν_λ	(930)		1290		ir		
		960	1290		R-p		A_1
		945	1300		ir		
ν_μ	(1160)						
		1558	2146	2090	ir		T_2
ν_ξ	1530	1562	2195		R-p		A_1
		1650	2207	2155	ir		T_2
		1929	2570		R-p		A_1
		1934	2581	2570	ir		T_2

^aNotation corresponds to Table II assignments; no implication of mode composition is intended.

^bAverage of similar frequency differences measured (see Table II). Values in parentheses are in doubt because of poor correspondence to $M(BD_4)_4$ spectra, low S/N , and/or infrequency of occurrence (see Sec. V).

^cReferences 13, 15, and 16 gas phase and Nujol solution data in ir, single crystal in Raman.

^dReference 14, short path length, low pressure, gas phase ir data.

^eFor $Hf(BH_4)_4$, $Hf(BD_4)_4$: R—room temperature single crystal Raman, R-p—polarized band in Raman, ir—gas phase, room temperature, or Nujol solution, room temperature infrared band.

^fThese assignments are meant only as possible (educated guesses of) symmetries for the $M(BH_4)_4$ vibrations causing the observed band. They derive: A_1 from R-p band, T_2 from intense ir bands, E from no Raman-ir overlap, and A_2, T_1 from simple energy considerations (see Sec. V).

structure seems to correspond with our preliminary normal coordinate analysis.¹³

In addition, the possibility that some of the weak assigned electronic origins may well be vibronic origins cannot be completely eliminated even in the absence of hot band intensity at 77 °K.

VI. ELECTRONIC ENERGY LEVEL CALCULATIONS

For actinide 4+ ions, crystal field interactions cannot be treated as a perturbation on intermediate coupling states; simultaneous diagonalization of electron–electron repulsion, spin orbit coupling, and crystal field interactions prove necessary.¹⁷ Using the readily available tabulations for these matrix elements,^{18,19} energy levels and eigenstates can be computed for any set of free ion and crystal field parameters. Modern statements of this procedure and its weak and strong points can be found in books by Judd and Wybourne.²⁰

The main problem encountered in attempting to apply this relatively standard actinide calculational scheme to U(BH₄)₄ experimental spectra is one of choosing near correct starting parameters for a least squares type fit of calculated to observed energy levels. Reasonable “first guess” free ion parameters can be taken from previous work on U⁴⁺ in hexahalide^{17a} and zircon²¹ environments. These parameters should change only slightly for U(BH₄)₄. Initial “free ion” parameters used were: Slater integrals, $F_2 = 185 \text{ cm}^{-1}$, $F_4 = 37 \text{ cm}^{-1}$, $F_6 = 3.7 \text{ cm}^{-1}$, and spin orbit coupling $\xi_{5f} = 1780 \text{ cm}^{-1}$.

Determination of starting values for cubic crystal field parameters,²² A ($\equiv A_{40}\langle r^4 \rangle$) and B ($\equiv A_{60}\langle r^6 \rangle$), however, is more complex. Qualitatively, the crystal field is expected to be large; how much larger than previously found for U⁴⁺ systems is not clear, nor is it obvious how this increased size should be expressed in terms of A and B . A point charge calculation for four ligands at corners of a regular tetrahedron [B(4)] results in a negative A and positive B . Using Lenander's values²³ of $\langle r^4 \rangle = 5.0 \text{ a.u.}$ and $\langle r^6 \rangle = 24.4 \text{ a.u.}$ and a U–B distance of 2.52 \AA ($r_{\text{U-B}(T)}$),⁷ a ratio of -0.11 is obtained for B/A . But, if instead the 12 hydrogen positions are considered for a point charge crystal field model [H(12)] (roughly corresponding to twelve charges at the midpoints of the edges of a cube), both A and B are negative and $B/A = 0.38$ ($r_{\text{U-H}} = 2.3 \text{ \AA}$).^{7c} Combining the two models gives B/A positive (A always negative) unless the charge at hydrogen positions is assumed to be very much less than that at the boron position ($|q_{\text{B}}| > 6|q_{\text{H}}|$). A combined model with $3|q_{\text{H}}| > |q_{\text{B}}|$ would seem reasonable if borohydride group bonding to uranium is via hydrogen bridges.

While it is possible to develop a prejudice for

one set of parameters, it was thought best to consider the question of proper starting parameters for the crystal field interaction to be largely unresolved. Plots of energy levels vs increasingly negative A values were made for several different B/A ratios, both negative and positive. These plots were then compared to experimental data to guess appropriate starting values for the least squares data fit process.

Since it has been observed that, even for rare earth ionic crystals, electrostatic point charge crystal field models do not always give the correct signs for experimental parameters,²⁴ plots of energy levels vs crystal field strength for positive A and B/A negative and positive were also constructed and compared to the observed spectra. Applicability of such plots are discussed in the following section.

VII. ASSIGNMENT OF ELECTRIC DIPOLE ORIGINS TO CALCULATED ENERGY LEVELS

The above discussed energy level diagrams admit only three possible ground states in T_d symmetry, A_1 , E , and T_2 —all predominantly ³H₄ in character. Of these, only T_2 is paramagnetic and, as the ground state, it should have a g value of ~ 2 . The considerable effort expended to observe a $g = 2$ EPR spectrum has not yielded reproducible signals with $S/N > 1$.

The absence of an EPR spectrum for U(BH₄)₄ over a wide range of conditions can be accounted for in several ways; the first and most obvious being that A_1 or E , not T_2 , is the ground state. Such a possibility will be considered further below.

A second reason could be that the T_d ground state is T_2 but that the molecule is distorted in the crystal at low temperatures. A large distortion would be ruled out from the relatively few observed $E1$ transitions (even in sites of D_{2d} , S_4 , or C_{3v} symmetry many more transitions would be allowed) and from the spectral continuity from gas phase to mixed crystal. Infrared vibrational results,¹⁴ leave little doubt that gas phase U(BH₄)₄ molecules are isostructural with T_d Hf(BH₄)₄. Since Hf(BH₄)₄ is still T_d at 24 °K⁶ and since no splittings or new features are observed in absorption between 77 and 2 °K, it is highly unlikely that the host crystal induces (or would even allow) a large distortion in the guest at low temperatures. Another important consideration in the elimination of a moderately distorted T_2 ground state is the lack of hot bands in the 77 °K spectrum.

Of course, a small distortion, causing the T_2 to split by only a few wavenumbers, cannot be eliminated from considerations of the optical spectrum alone due to linewidths. The full width at half-height (FWHH) for the sharper origins (5932, 16357,

17 622, and 20 694 cm^{-1}) varies from 6 to roughly 25 cm^{-1} at 2 °K. But, for such small splittings, second order Zeeman effects would be important at 93 kG. These would further split the T_2 state causing only its lowest component to be populated at 2 °K. This population change would give a blue shift to all transitions, which is inconsistent with observed spectra. Hence, it is maintained that a distorted T_2 ground state is ruled out by both temperature and Zeeman effects.

A third possible reason for the lack of EPR is that the sample saturates too easily or, conversely, that it relaxes too fast to be observed. Experiments using incident microwave powers as low as 2 μW and temperatures as low as 2 °K still did not indicate an absorption. Such proposed difficulties in the detection of EPR are thus unlikely but are, of course, not completely eliminated. In addition, sample concentrations were $\geq 0.1\%$ (known from optical absorption strengths) and therefore the number of U(IV) centers in the cavity was greater than 10^{17} for a typical experiment. Even at low powers, this is well within detectability for a moderately narrow line, ~ 100 G, and computed magnetic dipole matrix elements. But, more importantly, regardless of the specific EPR related hypotheses for such a state, its effects as a $g=2$ ground state will still be observable in the Zeeman spectrum. Simply stated, if $g \sim 2$ for the ground state, all transitions to higher states except those having very specific g values (+2 for T_1 and -2 for T_2) will be blue shifted due to the changing populations of the ground state components. At 4 °K and 93 kG, this shift is roughly 9 cm^{-1} —easily detectable on the previously mentioned sharp features of the visible spectrum. Indeed, several early efforts to assign the spectrum with a T_2 ground state, in both H(12) and B(4) models, yielded calculated Zeeman patterns for these states which predicted easily detectable shifts at low temperature and high field.⁴

Elimination of a T_2 ground state by the lack of EPR and by the Zeeman results forces consideration of A_1 and E . It should be noted here that Zeeman effect data are consistent with either an E or A_1 ground state (E is not Zeeman split to first order in the cubic group) and concomitant small excited state g values. However, referring to Table I and Fig. 9, it is clear that an A_1 ground state would allow only 10 or 11 electric dipole transitions in the region observed, 5000–30 000 cm^{-1} . All calculations leading to an A_1 ground state, based on physically reasonable parameters, fail to give enough T_2 , electric dipole allowed, states in the visible region to explain the major origins of the $\text{U}(\text{BD}_4)_4$ spectrum. These origins (at least 11) have Franck-Condon integrated oscillator strengths be-

tween 5×10^{-6} and 10^{-4} . Calculated magnetic dipole oscillator strengths for the various T_1-A_1 transitions are, in general, less than 1×10^{-6} and are typically less than 10^{-7} for transition energies greater than 12 000 cm^{-1} ; this would tend to eliminate T_1 states from explaining the spectrum with an A_1 ground state. Vibronically induced origins are also expected to be quite low in intensity, $f < 10^{-7}$, but for this molecule it is not inconceivable that they might be enhanced somewhat. Such a novel explanation for the strong states is eliminated by the lack of hot bands in the spectrum as the sample is warmed from 2 to 300 °K. Hence the A_1 ground state must be eliminated because it gives a low density of possible intense electric dipole transitions. An A_1 ground state model fails to explain even the strong origins, let alone the many weaker ones also proposed in Table II.

Thus, on the basis of Zeeman effect data, the lack of EPR data, and the density of transitions observed, it is concluded by a process of elimination that the ground state is $E(^3H_4)$.²⁵ Signs of crystal field parameters that lead to an E ground state are A and B both negative [H(12) model] and a model with A positive and B negative. The B(4) model with $A(-)$ and $B(+)$ and an "octahedral" model with $A(+)$ and $B(+)$ are therefore ruled out.

Excited electronic origins must be assigned by means of calculated energy level diagrams. To determine the initial size of crystal field parameters needed for calculations, two considerations seem most important: an E ground state and a roughly even distribution of states from 5000 to 25 000 cm^{-1} (as opposed to the distinct clustering of crystal-field-split intermediate coupling states that is found in rare earth ion crystal spectra). From comparison of several energy level plots for the H(12) model, it is found that $|B/A| < 0.8$ is needed to give the correct ground state along with an appropriate number of excited states within the experimentally accessible energy interval. Similarly, $|B/A| > 0.2$ is needed to avoid clustering of energy levels.

All plots within the range $0.2 \leq |B/A| \leq 0.8$ having both positive and negative values of B show the lowest T_1 originating from 3H_5 , $T_1(^3H_5)$, to have a small and negative crystal field dependence, to be located close to 6000 cm^{-1} , and to be at least 1000 cm^{-1} above the next excited state, $T_2(^3F_2)$. These plots also give $T_2(^3P_2)$ as the highest energy state below $A_1(^1S_0)$. [$A_1(^1S_0)$ is calculated to be in the vicinity of 40 000 cm^{-1} which is in the charge transfer/ $f-d$ transition region and is not observed.] The $T_2(^3P_2)$ level has a steep energy dependence on crystal field with respect to the ground $E(^3H_4)$, its energy ranging from 23 000 to 30 000 cm^{-1} for A

values from 0 to -1000 cm^{-1} .

The observed $U(\text{BD}_4)_4$ origin at 5932 cm^{-1} is apparently separated from states below it in energy by more than 1500 cm^{-1} . It shifts slightly to the red upon deuteration and upon temperature decrease from 77 to 2°K . In addition, the origin found at 24795 cm^{-1} is separated from higher energy states by at least 8000 cm^{-1} and it has the largest blue shift of any origin upon deuteration. It thus seems quite reasonable to assign the lowest observed origin at 5932 cm^{-1} [$U(\text{BD}_4)_4/\text{Hf}(\text{BD}_4)_4$ at 2°K] to $T_1(a^3H_5)$ and the highest observed origin at 24795 cm^{-1} in the same sample to $T_2(^3P_2)$.

The situation for the $A(+)$ $B(-)$ model is not so well defined. In particular, the lowest observed state although still $T_1(^3H_5)$ always calculates to have a steep crystal field dependence. In addition, even such seemingly unphysical B/A values as 2 to 4 can mock the spectrum for low values of A . Such

a wide latitude of crystal fields demanded several different sets of assignments to test the applicability of this model. But, crystal field parameters $|B/A| = 0.5$ and $A = -500 \text{ cm}^{-1}$ give an appropriate energy difference between $T_1(a^3H_5)$ and $T_2(^3P_2)$; that is, in either model the same magnitude crystal parameters serve as a reasonable initial guess. Knowing appropriate values of A and B for the experimental $U(\text{BD}_4)_4$ situation, it is possible to assign other origins for the two different crystal field models, $H(12)$ and $A(+)$ $B(-)$ from the calculation.

After several successive least squares fits, reassignments, and the addition of new assignments it became clear that the $H(12)$ model gave a superior fit to the data. For $H(12)$ it was possible to assign up to 18 energy levels (of a possible 19) to a mean deviation²⁶ Δ of 158 cm^{-1} . These assignments, the calculated energy levels and g values (for T_1 and T_2 states) are given in Table IV. The

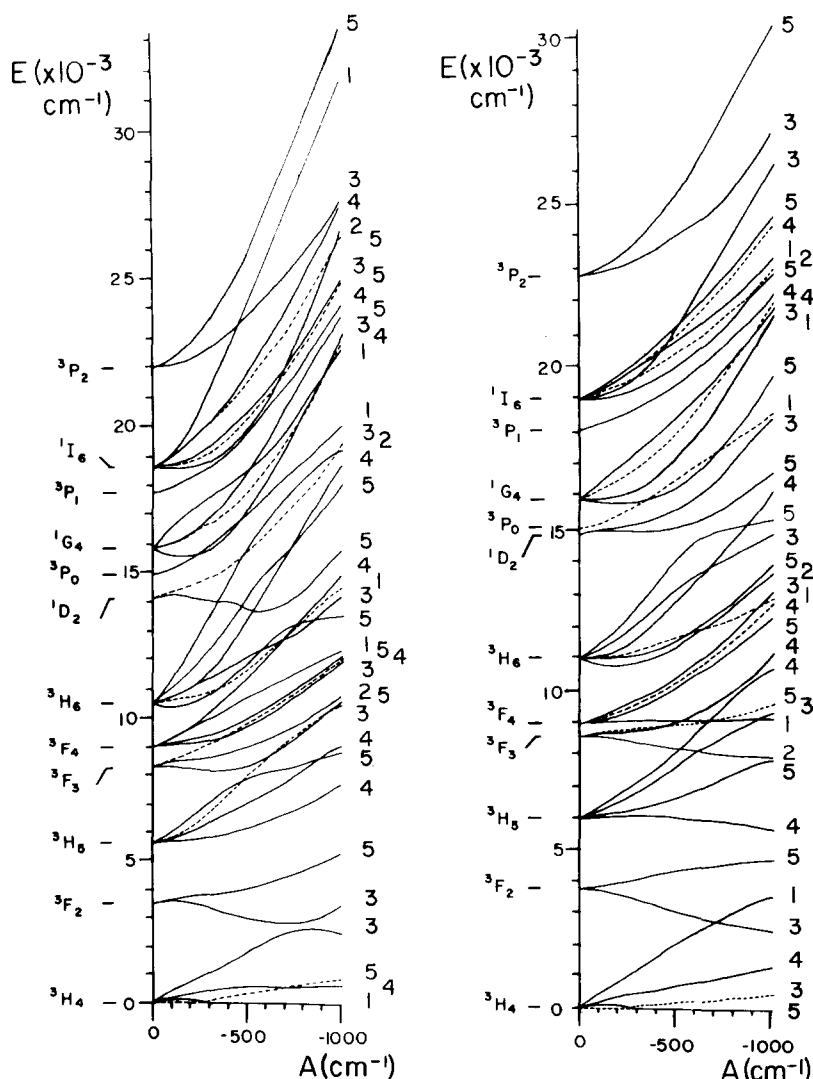


FIG. 9. Crystal field diagrams for $B(4)$ (left) and $H(12)$ (right) models. Plots are of transition energy ($\times 10^{-3} \text{ cm}^{-1}$) vs increasingly negative A (cm^{-1}) at $B/A = -0.73$ [$B(4)$] and $B/A = 0.55$ [$H(12)$]. Free ion parameters used are those from Ref. 21. Free ion levels are indicated in order of decreasing energy at $A = 0$ on the left of each diagram. 1S_0 is not included for convenience of illustration. Crystal field levels are indicated in order of decreasing energy at $A = -1000 \text{ cm}^{-1}$ on the right of each diagram: $1 \equiv A_1$, $2 \equiv A_2$, $3 \equiv E$, $4 \equiv T_1$, and $5 \equiv T_2$. Dotted lines are used merely to distinguish overlapping states and have no intrinsic meaning.

TABLE IV. Calculated energy levels and electronic origin assignments for $U(BD_4)_4$ in $Hf(BD_4)_4$.

State ^a	E_{calc} ^b	E_{obs} ^c	First order g value ^d	State ^a	E_{calc} ^b	E_{obs} ^c	First order g value ^d
$E(^3H_4)$	14	0		$E(^3H_6)$	12 913		
$T_2(^3H_4)$	0		1.95	$T_2(b-^3H_6)$	13 742	13 839	-2.23
$T_1(^3H_4)$	527		0.29	$T_2(^1D_2)$	14 915	(15 113)	-1.07
$A_1(^3H_4)$	1 833			$E(^1D_2)$	15 457		
$E(^3F_2)$	2 955			$A_1(^3P_0)$	15 625		
$T_2(^3F_2)$	4 071		-0.71	$T_2(^1G_4)$	16 038	(16 357) (16 057) ^e	2.18 ^f
$T_1(a-^3H_5)$	5 947	5 932	-0.79	$A_1(^1G_4)$	16 737		
$T_2(^3H_5)$	6 469	(6 735)	-2.13	$T_1(^1G_4)$	17 680	17 622	0.37 ^f
$E(^3H_5)$	7 510			$E(^1G_4)$	18 044		
$T_1(b-^3H_5)$	7 837	7 809	1.53	$T_1(^3P_1)$	18 302	18 280	1.43 ^f
$A_2(^3F_3)$	7 875			$T_2(a-^1I_6)$	19 900	(19 836)	-2.33
$T_1(^3F_3)$	8 784	(8 529)	-0.92	$A_2(^1I_6)$	20 340		
$T_2(^3F_3)$	8 867		1.36	$A_1(^1I_6)$	20 548		
$A_1(^3F_4)$	8 928			$T_2(b-^1I_6)$	20 624	20 694	-0.56 ^f
$T_2(^3F_4)$	9 782	(9 589)	1.10	$T_1(^1I_6)$	20 761	20 771	0.50
$T_1(^3F_4)$	10 100	(10 080)	0.43	$E(^1I_6)$	20 863		
$E(^3F_4)$	10 125			$E(^3P_2)$	23 355		
$A_2(^3H_6)$	11 196			$T_2(^3P_2)$	24 860	24 795	-0.85
$T_2(a-^3H_6)$	11 380	11 381	0.31	$A_1(^1S_0)$	41 354		
$A_1(^3H_6)$	11 434						
$T_1(^3H_6)$	12 490	12 528	0.15				

^aState symmetry designation explained in Ref. 5.

^bCalculated values from parameters listed in Table V, column 2, best fit to the 11 major $U(BD_4)_4$ states.

^cAssigned origins in parentheses are less certain and when added give a mean deviation of 158 cm^{-1} with parameters in column 3, Table V—the $U(BD_4)_4$ 18 assignment fit.

^dFirst order g values equal to $\langle T(+)|L_z+2S_z|T(+)\rangle$ were calculated using eigenvectors from the $U(BD_4)_4$ best 11 fit.

^eIf the weaker $16\,057\text{ cm}^{-1}$ origin is substituted for $16\,357\text{ cm}^{-1}$, the fit improves to $\Delta=135\text{ cm}^{-1}$.

^fSecond order effects on the g values for these four states were investigated. For all but one, $20\,694\text{ cm}^{-1}$, such effects were found to be negligible. In the $T_2(b^1I_6)$ state, mixing with the $T_1(^1I_6)$ at 100 kG reduces the magnitude of the expected g value by about 10%.

11 major assignments, corresponding to the more intense and well characterized origins, are indicated in Table IV. These fit to $\Delta=69\text{ cm}^{-1}$ with very similar final parameters which are listed in Table V along with the 18 assignment best fit parameters.

The best fit for these same 11 states in the $A(+)$ $B(-)$ model gave $\Delta=262\text{ cm}^{-1}$. The maximum number of assignments possible in this model was only 15 giving $\Delta=340\text{ cm}^{-1}$. The most severe shortcoming for the $A(+)$ $B(-)$ model is its inability to represent the 6000 cm^{-1} region in line position and crystal field dependences. Being relatively isolated, these transitions should be fit well in a crystal field approach. In addition, the best fit parameters for the $A(+)$ $B(-)$ model are distinctly un-

physical in that the F_4 value is nearly twice as large as would be predicted based on calculated F_4/F_2 ratios.²³ The conclusion drawn is that the $H(12)$ model with an E ground state is the only viable "crystal field" explanation of all the data.

From these assignments for $U(BD_4)_4$, in the $H(12)$ model, assignments for $U(BH_4)_4$ can be made. Here the maximum number of origins assigned is only 15, but comparison of the fits of the major 11 assignments in both hydride and deuteride can be made. The results are presented in Table V. If, for the 11 assignment $U(BH_4)_4$ fit, the free ion parameters are held fixed at the $U(BD_4)_4$ values, the best fit crystal field values do decrease slightly. It is interesting to note that for both the hydride and deuteride calculations, the first excited state

TABLE V. Final least squares fit parameters.

	U(BD ₄) ₄		U(BH ₄) ₄		
	11 Assignments	18 Assignments	11 Assignments	11 Assignments ^a	15 Assignments
F_2	186.7	187.3	186.2	•••	187.8
F_4	34.6	34.3	34.2	•••	35.9
F_6	3.81	3.85	3.78	•••	3.94
ζ_{5f}	1910.8	1937.8	1908.9	•••	1908.0
A	-435.5	-408.6	-436.7	-430.2	-371.9
B	-265.0	-252.5	-260.5	-259.2	-261.6
Δ^b	69	158	124	94	160

^aFor this fit to 11 U(BH₄)₄ states, the free ion parameters were held at the U(BD₄)₄ values and only the crystal field parameters were allowed to vary.

^bSee Ref. 26 for definition.

is $T_2(^3H_4)$, calculated to lie quite low in energy.

Calculated differences between U(BH₄)₄ and U(BD₄)₄ parameters fit in well with physically expected trends and generally account for H to D shifts tabulated in Table II.

VIII. DISCUSSION

A. Free Ion Parameters

From the foregoing interpretation of the U(BH₄)₄ cubic spectrum, it is not at all clear what effect covalency has on free ion parameters. In the H(12) model, little effect of covalency seems evident on F 's, although F_2 does decrease slightly while ζ_{5f} increases over that found for hexahalides. There appears to be no obvious explanation for this increase in ζ_{5f} , nor for the apparent lack of covalency effects on radial integrals. It should be remarked, however, that in a situation for which the model of a free ion in a crystal field is breaking down, there are undoubtedly interactions left out of the parameterized problem for which the included parameters, via a least squares refinement process, must compensate. The most obvious improvement in the model is a consideration of configuration interaction, especially with low lying charge transfer and $f-d$ states. One might also consider treating spin orbit coupling in a cubic, as opposed to a central, field.²⁷ While at present there appear to be insufficient assignments to justify inclusion of many more parameters, we are investigating addition of 2 more parameters in the form of configuration interaction.

It is perhaps best to consider that theoretical calculation of transition energies is simply a six parameter least squares analysis of the experimental results. It gives such surprisingly good results because the function chosen to which the data are fit has the tensorial form appropriate to the largest interactions.

B. Crystal Field

The crystal field contribution is also not very much larger than expected. The sixth order parameter B is large but not unlike that which might be predicted from the zircon results.²¹ In both cases, U(BH₄)₄ and U⁴⁺/ZrSiO₄, the uranium ion has many near neighbors; such relative increase of higher order crystal field parameters might be associated with the closer approach to spherical symmetry.

C. Vibrations

In general, intensity of vibrational structure following each electronic origin seems to follow the simple decreasing Franck-Condon envelope expected for small shifts in equilibrium geometry between electronic states (see Figs. 4 and 8). Vibrational frequencies observed in the absorption do not differ greatly (< 5%) from one electronic state to another. It is interesting to note that, in contrast to earlier work on hexahalides, vibrational frequencies of different electronic states appear to exhibit measureable changes. Unfortunately, the experimental error does not allow positive confirmation of frequency changes with electronic state. It would thus be premature to draw any implications concerning $5f$ electron involvement in borohydride bonding from this, but it seems clear from the amount of vibrational intensity that these electrons are not isolated from their molecular environment. A normal coordinate analysis¹³ should aid interpretation of these vibrational frequencies in excited electronic states.

D. Intensities

Individual peak intensities are of the order of $f \leq 10^{-5}$, which is roughly that expected for $4f$ forced electric dipole transitions.²⁸ This relatively low intensity may in part be due to the near O_h symmetry possessed by the 12 hydrogen atoms, leaving

most of the electric dipole intensity to be induced by the strictly T_d symmetry of the four boron atoms. Relative intensities are determined by admixtures of different configurations in the various crystal field states induced by odd terms in the crystal field. Actinide intensity calculations are usually quite inadequate and no attempt has been made at this time to calculate forced electric dipole oscillator strengths.

In a few transitions (e.g., 20 694, 20 771, 17 622, 13 831, and 5932 cm^{-1}), total intensity can be as much as an order of magnitude greater than the origin intensity if vibrational additions to the origin are also included in the calculation. Some of the weaker T_1 and T_2 origins ($f \sim 10^{-7}$) may well have magnetic dipole character in addition to their electric dipole intensity. Since the vibronic structure, both totally symmetric and nontotally symmetric, on assigned $E1$ crystal field electronic origins is so rich it is quite likely that some of the weaker origins, especially those given in Table II and not assigned by the calculations, are vibronically induced.

E. Hydride vs Deuteride Spectra

The differences in $\text{U}(\text{BH}_4)_4$ and $\text{U}(\text{BD}_4)_4$ spectra are the key to understanding them. Origin shifts correlate well to increases of crystal field from hydride to deuteride. Certainly some of the observed shift could be due to change in zero point energies of ground and excited state, but previous comments regarding small vibrational frequency changes upon electronic excitation indicate that this effect is probably not dominant. Interestingly enough, if $\text{U}(\text{BD}_4)_4$ "free ion" parameters (F_k 's and ζ_{5f}) are held fixed for $\text{U}(\text{BH}_4)_4$, the crystal field does indeed decrease. Added support for this assessment of H to D origin shifts as associated with increasing crystal field is the correlation of temperature effects (contraction of the lattice upon cooling) with deuteration effects for most observed origins.

Line shapes and widths differ widely in spectra of hydride and deuteride mixed crystals. There are also large variations within each one. While there appear to be no obvious explanations for why hydride spectra are much broader than deuteride spectra, it is possibly related to greater amplitude motion and anharmonicities present in hydride vibrational motion. Relative line broadening for a given crystal system is sometimes due to overlap of transitions and, in regions of high electronic and vibronic density of states, vibronic coupling may also give rise to increased linewidths.

F. Missing or Unassigned Origins and States

All origins of relative intensity greater than about 10–20 (see Table II) have been accounted for in the

least squares fit with the notable exception of 10 416 cm^{-1} (origin j , Table II). There appears to be no particular assignment possible for this feature as an origin. Since it has a rather strange H to D and temperature shift pattern, however, it may be due to some complicated overlap of effects. The possibility that this feature could be a vibronic origin has not been overlooked, but since no clearly obvious hot band intensity has been observed in this (or any other) region between 2 and 300 °K and since the H–D shift is blue while the 77 – 2 °K shift is red, such an explanation is considered unlikely.

In an attempt to find other states of the ground manifold, in particular $T_2(^3H_4, g \approx 2)$ and $T_1(^3H_4, g \approx 0.5)$, EPR spectra were looked for in the temperature range 2–30 °K (at $g \approx 2$) and at 77 °K (for all available fields). It is possible that if the $T_2(^3H_4)$ g is not equal to 2, its EPR signal at moderately low (6–30 °K) temperatures might not have been detected. On the other hand, samples initially at 4 °K scanned over a wider field range after the liquid helium boiled out of the cavity again indicated no new signals as the sample warmed. The fact that no signals were observed, coupled with small Zeeman effects and no hot band features, indicates the E ground state is separated from the next electronic crystal field state by probably more than 100 cm^{-1} . Thus, the T_1 and T_2 components of the ground term are probably well embedded in the rather dense vibronic manifold within 110 cm^{-1} of the electronic ground state (see, for example, the 6000 cm^{-1} region in Fig. 4). These vibrational modes, together with the large vibrational amplitudes of the BH_4 groups should cause fast spin–lattice relaxation times and thus very weak broad EPR spectra. The density of energy levels beginning at about 100 cm^{-1} up from the ground state may also account for the observed absence of hot band features and the monotonic structureless increase in linewidth with increasing temperature.

G. Further Experimentation

A fuller understanding of $\text{U}(\text{BH}_4)_4$ should result from emission spectra which could give data on low lying energy levels and, via selection rules, give weight to some of the less certain assignments. Search for emission is presently under way in both the visible and near infrared regions.

Zeeman data in the near ir would be quite useful in this system because lines in the 6000 cm^{-1} region are the sharpest observed ($\sim 6 \text{ cm}^{-1}$ at 2 °K). Small shifts and splittings expected in this region should be observable as such with available resolution. Magnetic circular dichroism could also be used to enhance resolution of magnetic field effects throughout the spectra.

Resonance Raman experiments could aid in confirmation of vibrational interactions important in these states although intensity enhancement would be small. Raman scattering due to low lying electronic states should also be helpful in finding new origins to test the crystal field model. Both types of Raman experiments are planned in an effort to get more physical data to confirm assignments that must now rest heavily on calculational grounds.

IX. CONCLUSIONS

The data presented here point quite clearly to the conclusion that uranium borohydride spectra are indicative of a molecule. A mixed crystal of $U(BH_4)_4$ in either $Zr(BH_4)_4$ or $Hf(BH_4)_4$ can certainly be classified as a molecular crystal.

In some sense it is surprising that any crystal field model can fit the observed transitions to about 100 cm^{-1} , especially in a molecule. It is clear that "covalency" is a complex phenomenon and that central ion-point charge electrostatic models break down in involved ways. Configuration interaction, shielding, overlap, and exchange must all play a role in making the integrals F_2 , F_4 , F_6 , ζ_{5f} , A , and B simply experimental parameters in an effective Hamiltonian. Even such complications as electron correlation, cubic spin orbit coupling, and 2 electron potentials, in part, can contribute to the Hamiltonian with the same transformation properties as the above six parameters.

ACKNOWLEDGMENT

We wish to thank Professor D. S. McClure for helpful discussions concerning crystal field models.

*Work supported in part by the Office of Naval Research, the National Science Foundation, and the U.S. Army Research Office-Durham.

†Part of this work was performed while the authors were Guest Scientists at the Francis Bitter National Magnet Laboratory, which is supported at MIT by the National Science Foundation.

‡National Science Foundation Predoctoral Fellow, 1969-1972.

¹General reviews of pure crystal exciton theory are found in: (a) A. S. Davydov, *Usp. Fiz. Nauk* **82**, 393 (1964); [*Sov. Phys.-Usp.* **7**, 145 (1964)]; *Theory of Molecular Excitons* (McGraw-Hill, New York, 1962 and Plenum Press, New York, 1971); (b) S. A. Rice and J. Jortner, in *Physics and Chemistry of the Organic Solid State*, edited by D. Fox *et al.* (Interscience, New York, 1967), Vol. III, p. 201; (c) G. W. Robinson, *Annu. Rev. Phys. Chem.* **21**, 429 (1970); (d) E. R. Bernstein, S. D. Colson, R. Kopelman, and G. W. Robinson, *J. Chem. Phys.* **48**, 5596 (1968).

²For a review of metal borohydrides see: B. D. James and M. G. H. Wallbridge, *Prog. Inorg. Chem.* **11**, 99 (1970).

³E. R. Bernstein and K. M. Chen (unpublished).

⁴E. R. Bernstein and T. A. Keiderling (unpublished results) and T. A. Keiderling, Thesis, Princeton University, 1973.

⁵D. R. Johnston, R. A. Satten, C. L. Schreiber, and E. Y. Wong, *J. Chem. Phys.* **44**, 3141 (1966).

⁶(a) P. H. Bird and M. R. Churchill, *Chem. Commun.* 403 (1967); (b) V. Plato and K. Hedberg, *Inorg. Chem.* **10**, 590 (1971); (c) E. R. Bernstein, W. C. Hamilton, T. A. Keiderling, W. J. Kennelly, S. J. LaPlaca, S. J. Lippard, T. J. Marks, and J. J. Mayerle (work in progress).

⁷(a) W. H. Zachariasen, Manhattan Project, Chicago Metallurgical Lab CP 3774, p. 17, 1946. (b) E. R. Bernstein, T. A. Keiderling, S. J. Lippard, and J. J. Mayerle, *J. Am. Chem. Soc.* **94**, 2552 (1972); (c) E. R. Bernstein, W. C. Hamilton, T. A. Keiderling, S. J. LaPlaca, S. J. Lippard, and J. S. Mayerle, *Inorg. Chem.* **11**, 3009 (1972).

⁸W. E. Reid, J. M. Bish, and A. Brenner, *J. Electrochem. Soc.* **104**, 21 (1957).

⁹H. I. Schlesinger and H. C. Brown, *J. Am. Chem. Soc.* **75**, 219 (1953).

¹⁰H. I. Schlesinger, H. C. Brown, and E. K. Hyde, *J. Am. Chem. Soc.* **75**, 209 (1953).

¹¹J. U. White, *J. Opt. Soc. Am.* **32**, 285 (1942).

¹²We wish to thank E. Wasserman, W. Yager, and R. S. Hutton at Bell Laboratories (Murray Hill) for the use of this equipment.

¹³E. R. Bernstein, R. S. Gay, D. Jurkowitz, T. A. Keiderling, S. J. Lippard, T. G. Spiro, and W. H. Wozniak (unpublished results).

¹⁴B. D. James, B. E. Smith, and M. G. H. Wallbridge, *J. Mol. Struct.* **14**, 327 (1972).

¹⁵T. J. Marks, W. J. Kennelly, J. R. Kolb, and L. A. Shimp, *Inorg. Chem.* **11**, 2540 (1972).

¹⁶N. Davies, D. Saunders, and M. G. H. Wallbridge, *J. Chem. Soc. A* 1970, 2915; B. D. James, R. K. Nanda, M. G. H. Wallbridge, *J. Chem. Soc. A* 1966, 182.

¹⁷(a) R. A. Satten, C. L. Schreiber, and E. Y. Wong, *J. Chem. Phys.* **42**, 162 (1965); (b) J. R. Clifton, D. M. Gruen, and A. Ron, *J. Chem. Phys.* **51**, 224 (1969).

¹⁸R. A. Satten and J. S. Margolis, *J. Chem. Phys.* **32**, 573 (1960).

¹⁹(a) E. U. Condon and G. H. Shortley, *Theory of Atomic Spectra* (Cambridge U. P., England, 1967); (b) C. W. Nielson and G. F. Koster, *Spectroscopic Coefficients for the p^n , d^n and f^n Configurations* (MIT Press, Cambridge, MA, 1963).

²⁰(a) B. R. Judd, *Operator Techniques in Atomic Spectroscopy*, (McGraw-Hill, New York, 1963); (b) B. G. Wybourne, *Spectroscopic Properties of Rare Earths*, (Interscience, New York, 1965).

²¹I. Richman, P. Kisliuk, and E. Y. Wong, *Phys. Rev.* **155**, 262 (1967).

²²M. T. Hutchings, *Solid State Phys.* **16**, 227 (1964).

²³C. J. Lenander, *Phys. Rev.* **130**, 1033 (1963); values derived from relativistic wavefunctions yield similar results: W. B. Lewis, J. B. Mann, D. A. Liberman, and D. T. Cromer, *J. Chem. Phys.* **53**, 809 (1970).

²⁴D. J. Newman, *Adv. Phys.* **20**, 197 (1971).

²⁵Notation characterizing a state by an irreducible representation and a multiplet symbol, $\Gamma_i({}^{2S+1}L_J)$, is meant to serve as a labeling device only. The multiplet designation merely implies the origin of that state on a crystal field plot; it does not signify the free ion level of maximum contribution to the eigenvector which actually describes the state.

²⁶Mean error, Δ , is defined as $[\sum_i^N e(E_i^c - E_i^e)^2 / (N_e - N_p)]^{(1/2)}$, where E_i^c are calculated energy levels, E_i^e and N_p is the number of parameters used in the least squares fit.

²⁷H. A. Buchmaster, R. Chatterjee, and Y. H. Shing, *Can. J. Phys.* **50**, 78 (1972); J. S. Griffith, *Theory of Transition Metal Ions* (Cambridge U. P., Cambridge, England, 1961).

²⁸B. R. Judd, *Phys. Rev.* **127**, 750 (1962); G. S. Ofelt, *J. Chem. Phys.* **37**, 511 (1962); W. T. Carnall, P. R. Fields, and B. G. Wybourne, *J. Chem. Phys.* **42**, 3797 (1965); and W. F. Krupke, *Phys. Rev.* **145**, 325 (1966).